Available online at www.sciencedirect.com
ScienceDirect
Journal of Solid State Chemistry 180 (2007) 3401–3407
JOURNAL OF SOLID STATE CHEMISTRY
www.elsevier.com/locate/jssc

# Magnetic and Mössbauer studies of 5% Fe-doped $BiMnO_3$

Alexei A. Belik[a,*], Naoaki Hayashi[b], Masaki Azuma[c], Shigetoshi Muranaka[b], Mikio Takano[c], Eiji Takayama-Muromachi[a]

[a]*Advanced Nano Materials Laboratory (ANML), National Institute for Materials Science (NIMS), 1-1 Namiki, Tsukuba, Ibaraki 305-0044, Japan*
[b]*Graduate School of Human and Environmental Studies, Kyoto University, Kyoto 606-8501, Japan*
[c]*Institute for Chemical Research, Kyoto University, Uji, Kyoto-fu 611-0011, Japan*

Received 5 July 2007; received in revised form 1 October 2007; accepted 2 October 2007
Available online 11 October 2007

**Abstract**

$^{57}$Fe Mössbauer spectroscopy, dc and ac magnetization, specific heat, and differential scanning calorimetry measurements were performed in a powder $BiMn_{0.95}Fe_{0.05}O_3$ sample prepared at 6 GPa and 1383 K. The substitution of 5% Fe for Mn increases the temperatures of the structural monoclinic-to-orthorhombic phase transition (from 768 to 779 K) and the ferromagnetic transition (from 98 to 109 K) by about 10 K in $BiMn_{0.95}Fe_{0.05}O_3$ compared with $BiMnO_3$. On the other hand, the temperature of the monoclinic-to-monoclinic phase transition associated with the orbital ordering strongly decreases in $BiMn_{0.95}Fe_{0.05}O_3$ (414 K) compared with that of $BiMnO_3$ (474 K). The saturated magnetic moment at 5 K and 5 T is also suppressed from 3.92 $\mu_B$ per formula unit in $BiMnO_3$ to 3.35 $\mu_B$ in $BiMn_{0.95}Fe_{0.05}O_3$. The large quadrupole splitting (1.18 mm/s) observed at 293 K in $BiMn_{0.95}Fe_{0.05}O_3$ can be explained by the strong Jahn-Teller distortion and cooperative orbital order. The quadrupole splitting reduces by two times above the orbital melting temperature.


*Keywords:* Multiferroics; Fe-doped $BiMnO_3$; Mössbauer spectroscopy; Magnetic susceptibility

## 1. Introduction

$BiMnO_3$ is a well-established ferromagnetic insulator with the ferromagnetic Curie temperature $T_C = 99$–$103$ K [1–3]. $BiMnO_3$ has attracted a lot of interest as a multiferroic material [4,5]. The orbital degrees of freedom are active in $BiMnO_3$ resulting in the orbital-ordered state [6–8]. $BiMnO_3$ has a highly distorted perovskite-type structure at room temperature and crystallizes in a monoclinic system [2,6,8]. $BiMnO_3$ undergoes two high-temperature phase transitions at $T_{OO} = 474$ K and $T_{str} = 768$ K [3,8]. The phase transition at 474 K is a monoclinic-to-monoclinic phase transition without any detectable change in the symmetry accompanied by a thermal effect, abrupt changes of lattice parameters and unit cell volume, a small jump of resistivity and magnetization, and an anomaly of dielectric constant [3,8–10]. Structural analysis from neutron powder diffraction data allowed us to suggest that this phase transition corresponds to the orbital ordering (OO) [8]. The phase transition at 768 K is a structural (str) monoclinic-to-orthorhombic transition [3].

The doped $Bi_{1-x}M_xMnO_3$ ($M$ = Ca and Sr) samples demonstrate different transitions with charge and orbital orders [11]. We have recently investigated solid solutions $BiMn_{1-x}M_xO_3$ with $M$ = Al, Sc, Cr, Fe, and Ga and effects of isovalent substitution in the Mn sublattice on magnetic, thermal, and structural properties of $BiMnO_3$ [12–14]. The orbital order in $BiMnO_3$ was found to be very fragile. It disappears at the doping level of 0.02–0.08. There are other works on the $BiFeO_3$–$BiMnO_3$ system, but they mainly describe the results in the vicinity of $BiFeO_3$ [15–19].

Mössbauer spectroscopy can provide useful information about the local structure and magnetic interactions. To the best of our knowledge, there are no Mössbauer spectroscopy studies on $BiMnO_3$ and related compounds except for mechanosynthesized $BiFe_{1-x}Mn_xO_3$ ($x = 0.5$) [15]. On

*Corresponding author. Fax: +81 29 860 4706.
*E-mail address:* Alexei.BELIK@nims.go.jp (A.A. Belik).

0022-4596/$ - see front matter © 2007 Elsevier Inc. All rights reserved.
doi:10.1016/j.jssc.2007.10.006

the other hand, Mössbauer spectroscopy has been applied to study stoichiometric, cation-deficient, and doped $LaMnO_3$ samples [20,21] that show rich and important physical properties such as colossal magnetoresistance [22,23], different charge- and orbital-ordered states [24], and metal–insulator transitions [24,25]. In $LaMnO_3$, the orbital ordering takes place below $T_{OO} = 750$–$780$ K, and the antiferromagnetic ordering below $T_N = 140$ K [26–28].

In this work, we present detailed characterization of $BiMn_{0.95}Fe_{0.05}O_3$ using dc and ac magnetization, specific heat, and differential scanning calorimetry (DSC) measurements. We also report $^{57}$Fe Mössbauer data of $BiMn_{0.95}Fe_{0.05}O_3$ at different temperatures below and above the orbital ordering temperature $T_{OO}$ and ferromagnetic temperature $T_C$.

## 2. Experimental

A stoichiometric mixture of $Bi_2O_3$ (99.99%), $Mn_2O_3$, and $^{57}Fe_2O_3$ ($^{57}$Fe 95.5%) was placed in Au capsules and treated at 6 GPa in a belt-type high-pressure apparatus at 1383 K for 60 min (heating rate 110 K/min). After heat treatment, the sample was quenched to room temperature (RT), and the pressure was slowly released. The resultant sample was black powder. Single-phased $Mn_2O_3$ was prepared from a commercial $MnO_2$ (99.99%) by heating in air at 923 K for 24 h. X-ray powder diffraction (XRD) data of $BiMn_{0.95}Fe_{0.05}O_3$ collected at RT on a RIGAKU Ultima III diffractometer using Cu$K\alpha$ radiation ($2\theta$ range of 8–95°, a step width of 0.02°, and a counting time of 13 s/step) showed that the samples contained very small amount (1.1 mass%) of $Bi_2O_2CO_3$ as an impurity. The lattice parameters were refined by the Rietveld method with RIETAN-2000 [29] ($a = 9.5355(3)$ Å, $b = 5.6103(2)$ Å, $c = 9.8530(3)$ Å, and $\beta = 110.474(2)°$). The value of the $\beta$ angle suggests that $BiMn_{0.95}Fe_{0.05}O_3$ is in the orbitally ordered state [8,12].

The dc magnetic susceptibilities, $\chi = M/H$, of $BiMn_{0.95}Fe_{0.05}O_3$ were measured on a SQUID magnetometer (Quantum Design, MPMS) between 2 and 350 K in applied fields of $10^{-2}$ and 1 T under both zero-field-cooled (ZFC) and field-cooled (FC) conditions. The thermoremanent magnetization (TRM) curve was measured at zero magnetic field on heating after cooling the sample from 150 to 2 K at 0.1 T. Isothermal magnetization measurements were performed between −5 and 5 T at 5 K. Frequency-dependent ac susceptibility measurements at zero static magnetic field were performed with Quantum Design MPMS and PPMS instruments from 200 to 2 K at frequencies ($f$) between 0.5 and $10^4$ Hz and applied oscillating magnetic fields ($H_{ac}$) of $2.5 \times 10^{-5}$ and $5 \times 10^{-4}$ T. We also measured ac susceptibilities at zero static magnetic field and $f = 110$ Hz with different $H_{ac} = 0.05$, 0.25, 1, and $5 \times 10^{-4}$ T. Specific heat, $C_p$, of $BiMn_{0.95}Fe_{0.05}O_3$ at zero static magnetic field and 9 T was recorded between 2 and 300 K on cooling by a pulse relaxation method using a commercial calorimeter (Quantum Design PPMS). For the specific heat measurements, the powder $BiMn_{0.95}Fe_{0.05}O_3$ sample was cold-pressed at 1 GPa to make pellets. $^{57}$Fe Mössbauer spectra were measured with transmission geometry using a $^{57}$Co/Rh source (activity of about 800 MBq (an averaged value during about 6 months)). The sample weight for the Mössbauer measurements was about 50 mg, and the sample thickness was about 0.3 mm in an Al foil. A hand-made oven and a hand-made cryostat with liquid $N_2$ and He were used for measurements above RT and at 77 and 4.2 K. Obtained spectra were calibrated by α-Fe as a standard, and were fitted by Lorentzian function. DSC curves of $BiMn_{0.95}Fe_{0.05}O_3$ were recorded on a SII Exstar 6000 (DSC 6220) system at a heating/cooling rate of 10 K/min from 133 to 795 K in semi-closed aluminum capsules. The DSC runs were cycled between 300 and 620 K several times, then the sample was heated up to 795 K, and finally the DSC runs were cycled again between 300 and 620 K.

## 3. Results and discussion

The DSC curves of $BiMn_{0.95}Fe_{0.05}O_3$ and $BiMnO_3$ are given in Fig. 1. $BiMnO_3$ demonstrates two sharp peaks at $T_{OO} = 474$ K and $T_{srt} = 768$ K (on heating) [8,9,14]. The DSC data showed that the two high-temperature phase

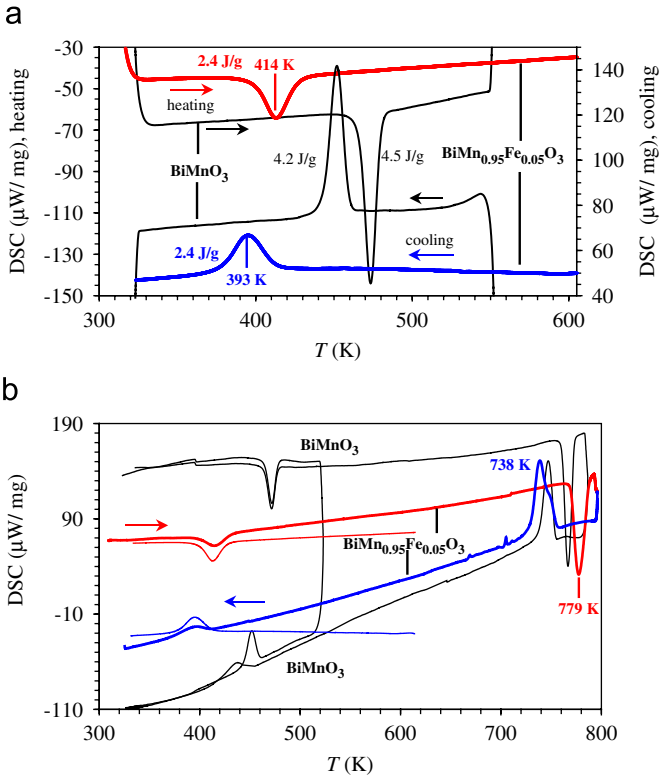


Fig. 1. Heating–cooling DSC curves of $BiMn_{0.95}Fe_{0.05}O_3$ during cycling (a) between 300 and 620 K and (b) between 300 and 620 K and 300 and 795 K. DSC curves of $BiMnO_3$ (from Refs. [8,14]) are given for comparison. The cycling between 300 and 620 K is duplicated in (b) to emphasize changes of the cooling curves after heating up to about 800 K.

transitions survive in $BiMn_{0.95}Fe_{0.05}O_3$ in comparison with $BiMn_{0.95}Sc_{0.05}O_3$, where the first phase transition is completely suppressed [14]. However, the temperature of the monoclinic-to-monoclinic transition in $BiMn_{0.95}Fe_{0.05}O_3$ strongly decreases by 60 K ($T_{OO} = 414$ K), while the temperature of the monoclinic-to-orthorhombic transition increases slightly by 9 K to $T_{srt} = 779$ K. The DSC anomalies of $BiMn_{0.95}Fe_{0.05}O_3$ at $T_{OO}$ are noticeably broadened, and the intensity is reduced compared with $BiMnO_3$. The cycling of the DSC curves of $BiMn_{0.95}Fe_{0.05}O_3$ between 300 and 620 K gives quite reproducible results with very small changes in the peak position and intensity. The magnitude of the latent heat was extracted from the peak areas (the values are given in Fig. 1a).

The change of the entropy (on heating) was estimated to be 3.04 J/(mol K) (33% of $R\ln 3$) in $BiMnO_3$ and 1.87 J/(mol K) (20% of $R\ln 3$) in $BiMn_{0.95}Fe_{0.05}O_3$. We will discuss about these values later. After heating $BiMn_{0.95}Fe_{0.05}O_3$ (and also $BiMnO_3$) up to 795 K, the phase transitions near $T_{OO}$ were significantly smeared during the cooling measurements (Fig. 1b). The XRD measurement after the DSC experiment showed that the phase composition of the $BiMn_{0.95}Fe_{0.05}O_3$ sample remained the same but the lattice parameters of $BiMn_{0.95}Fe_{0.05}O_3$ were slightly modified ($a = 9.5268(4)$ Å, $b = 5.6123(2)$ Å, $c = 9.8376(5)$ Å, and $\beta = 110.249(4)^\circ$ [12]). These facts may show that the oxygen content of $BiMn_{0.95}Fe_{0.05}O_3$ and $BiMnO_3$ changed after heating up to about 800 K or the samples just stated to decompose as in the case of $BiCrO_3$ [30] and some $BiMn_{1-x}M_xO_3$ [12].

Fig. 2 shows dc magnetic susceptibilities of $BiMn_{0.95}Fe_{0.05}O_3$ between 2 and 600 K. The transition to the ferromagnetic state in $BiMn_{0.95}Fe_{0.05}O_3$ is observed at $T_C = 109$ K as determined by the peak on the ZFC $d(\chi T)/dT$ vs $T$ curve measured at 0.01 T. The ferromagnetic transition temperature increases by about 10 K compared with that of $BiMnO_3$. A pronounced irreversibility is observed between the ZFC and FC curves measured at 0.01 T. This irreversibility starts just below $T_C$. At the low magnetic field (0.01 T), additional anomalies are observed near 20 K on both ZFC and FC curves. On the other hand, the ZFC and FC curves almost coincide with each other when measured at 1 T, and no anomalies are found. The inverse ZFC magnetic susceptibilities in the temperature ranges of 300–380 and 430–600 K are fit by the Curie–Weiss equation:

$$\chi(T) = \mu_{eff}^2 N(3k_B(T-\theta))^{-1}, \quad (1)$$

where $\mu_{eff}$ (4.588(4) $\mu_B$ at 300–380 K and 4.719(3) $\mu_B$ at 430–600 K) is effective magnetic moment, $N$ is Avogadro's number, $k_B$ is Boltzmann's constant, and $\theta$ (134.0(3) K at 300–380 K and 121.5(4) K at 430–600 K) is the Weiss constant. The effective magnetic moment of $BiMn_{0.95}Fe_{0.05}O_3$ slightly increases, and Weiss constant slightly decreases through $T_{OO}$ similar to $BiMnO_3$ [8]. However, the orbital melting in $BiMnO_3$ is accompanied by the step-like decrease of the $\chi^{-1}$ vs $T$ curve, and the temperature

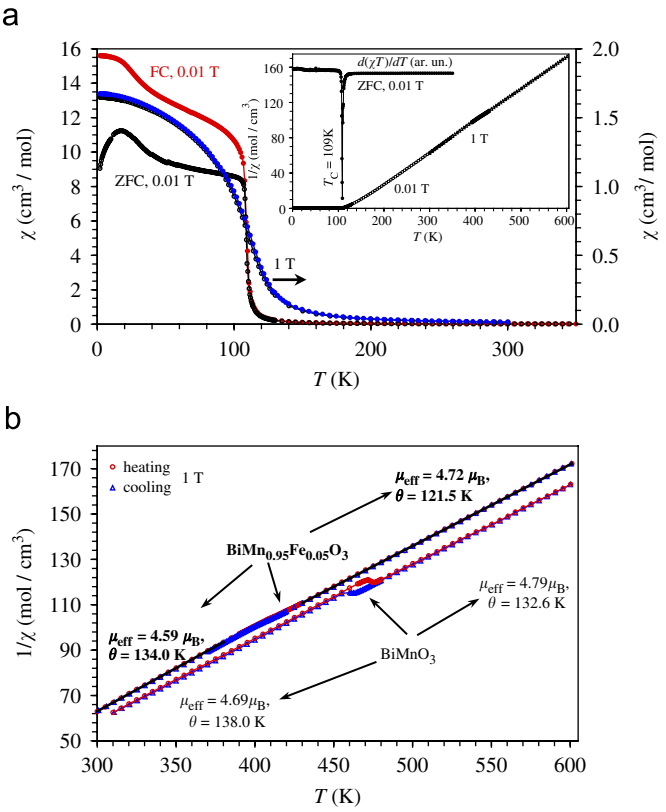


Fig. 2. (a) ZFC and FC dc magnetic susceptibility ($\chi = M/H$) curves of $BiMn_{0.95}Fe_{0.05}O_3$ measured at $10^{-2}$ and 1 T. The inset gives the ZFC $\chi^{-1}$ vs $T$ and $d(\chi T)/dT$ vs $T$ curves measured at 0.01 T. (b) The inverse magnetic susceptibilities measured at 1 T for $BiMn_{0.95}Fe_{0.05}O_3$ and $BiMnO_3$ (from Ref. [8]) between 300 and 600 K. The solid lines show the fits by the Curie–Weiss equation. The parameters, $\mu_{eff}$ and $\theta$, of the fits are given.

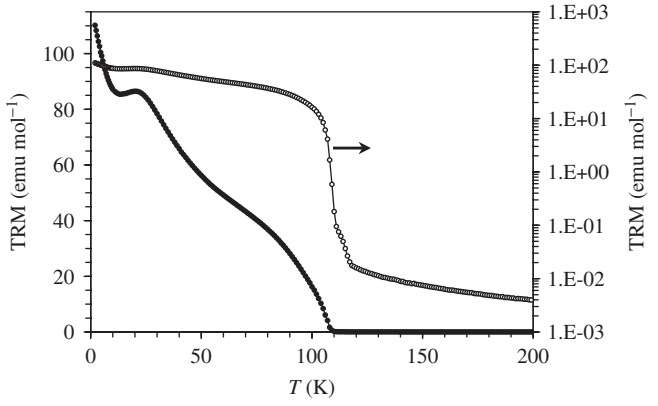


Fig. 3. Thermoremanent magnetization (TRM) curve as a function of temperature for $BiMn_{0.95}Fe_{0.05}O_3$. The TRM curve was measured at zero magnetic field on heating after cooling the sample from 150 to 2 K at 0.1 T. The secondary $y$-axis gives the same curve in the logarithmic scale.

hysteresis is observed. On the other hand, no step-like changes and no hysteresis was found in $BiMn_{0.95}Fe_{0.05}O_3$ on the $\chi^{-1}$ vs $T$ curves through the phase transition temperature $T_{OO}$. This fact can be explained by the significant smearing of the phase transition as indicated by the DSC results (Fig. 1a).

The TRM curve as a function of temperature is given in Fig. 3. After a noticeable decrease of the TRM from 2 to about 12 K, there is a small increase up to 20 K. Then, the TRM gradually decreases when approaching $T_C$. The logarithmic presentation clearly demonstrates the presence of an additional ferromagnetic contribution below 114 K. Note that a very small anomaly at 114 K was also observed in $BiMnO_3$ [10,31]. This anomaly was explained by the presence of a small amount of another perovskite-like modification [10].

Fig. 4 depicts the isothermal magnetization curves at 5 K. A very small hysteresis is observed with the coercive field ($H_c$) of about $25 \times 10^{-4}$ T and the remnant magnetization ($M_r$) of about $6.9 \times 10^{-2}\,\mu_B$ per formula unit. These values are slightly larger than those of the undoped $BiMnO_3$ ($H_c \approx 3 \times 10^{-4}$ T and $M_r \approx 1.3 \times 10^{-2}\,\mu_B$) [31]. The magnetic moment at 5 K and 5 T ($M_S$) is about 3.35 $\mu_B$ per formula unit. This value is smaller by 15% than that of $BiMnO_3$ ($M_S = 3.92\,\mu_B$) [31]. This reduction of $M_S$ can be explained if we assume that the incorporated $Fe^{3+}$ ions ($S = 5/2$, $S$ is spin) are coupled antiferromagnetically with the surrounding six $M^{3+}$ ($M$ = Mn and Fe) ions. Therefore, $BiMn_{0.95}Fe_{0.05}O_3$ should be considered as a random ferrimagnet. The saturated magnetic moment further decreases to 2.5 $\mu_B$ per formula unit in $BiMn_{0.85}Fe_{0.15}O_3$ [12], and 1.5 $\mu_B$ in $BiMn_{0.8}Fe_{0.2}O_3$ [13].

Fig. 5 shows the ac susceptibility curves of $BiMn_{0.95}Fe_{0.05}O_3$. Sharp peaks are observed near 108 K on the $\chi'$ vs $T$ and $\chi''$ vs $T$ curves indicating the onset of a ferromagnetic order. Additional broad anomalies are found near 98 K on both $\chi'$ vs $T$ and $\chi''$ vs $T$ curves and near 20 K on the $\chi'$ vs $T$ curve. The temperature of the latter anomaly coincides with the temperatures of the anomalies observed on the ZFC $\chi$ vs $T$ (0.01 T) and TRM curves. The anomalies similar to the former one were observed in $BiMnO_3$ at 84 K (Fig. 5) [31]. The temperature shift of about 14 K is close the temperature shift of $T_C$. This fact gives support that the anomalies at 84 K in $BiMnO_3$ and at 98 K in $BiMn_{0.95}Fe_{0.05}O_3$ are intrinsic, however, their origin is not clear. It should be noted that

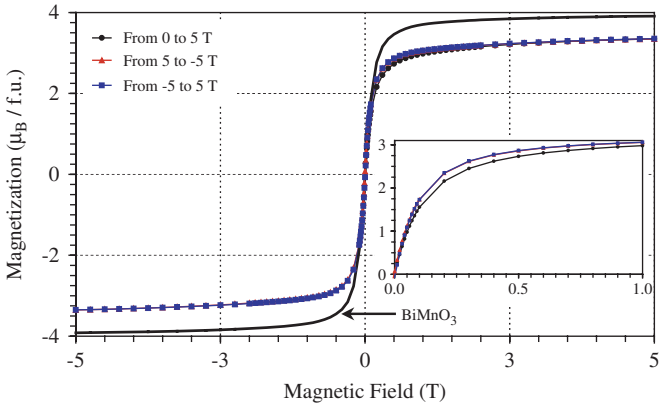


Fig. 4. Isothermal magnetization curves of $BiMn_{0.95}Fe_{0.05}O_3$ at 5 K. Inset shows the curves between 0 and 1 T. The $M$ vs $H$ curve of $BiMnO_3$ (from Ref. [8]) is given for the comparison.

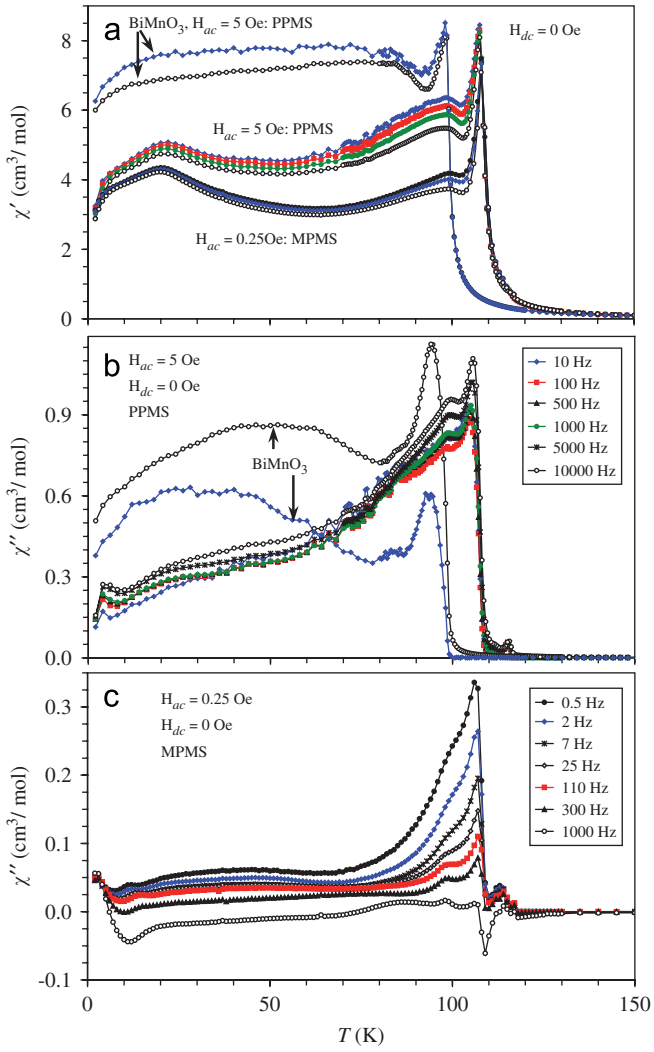


Fig. 5. Real $\chi'$ (a) and imaginary $\chi''$ (b and c) parts of the ac susceptibility as a function of temperature (2–150 K) for $BiMn_{0.95}Fe_{0.05}O_3$. Measurements were performed on cooling at zero static field using ac fields with the amplitude $H_{ac} = 2.5 \times 10^{-5}$ and $5 \times 10^{-4}$ T. The $\chi'$ vs $T$ and $\chi''$ vs $T$ curves of $BiMnO_3$ (from Ref. [31], at $H_{ac} = 5 \times 10^{-4}$ T and $f = 10$ and $10^4$ Hz) are given for the comparison in (a) and (b). For frequency values in (a) at $H_{ac} = 2.5 \times 10^{-5}$ and $5 \times 10^{-4}$ T, see parts (c) and (b), respectively.

clear anomalies are also found near 114 K on the $\chi''$ vs $T$ curves in agreement with the TRM curve.

Fig. 6 depicts the $\chi'$ vs $T$ and $\chi''$ vs $T$ curves at different oscillating fields $H_{ac}$. At low $H_{ac} = 5 \times 10^{-6}$ and $2.5 \times 10^{-5}$ T, the curves are very similar to each other. However, both components of the ac susceptibilities grow rapidly when the ac field further increases, especially, from 1 to $5 \times 10^{-4}$ T. These results may be explained by the pinning of domain walls because for higher $H_{ac}$ the domain wall are more responsive. At high $H_{ac}$ ($5 \times 10^{-4}$ T) when the ac field is able to alter the domain structure, very similar $\chi''$ vs $T$ curves are observed with weak dependence on frequency (Fig. 5b). On the other hand, at low $H_{ac}$ ($2.5 \times 10^{-5}$ T), the $\chi''$ vs $T$ curves are strongly suppressed with increasing frequency probably because the domain structure is hardly changed by application of low $H_{ac}$ with

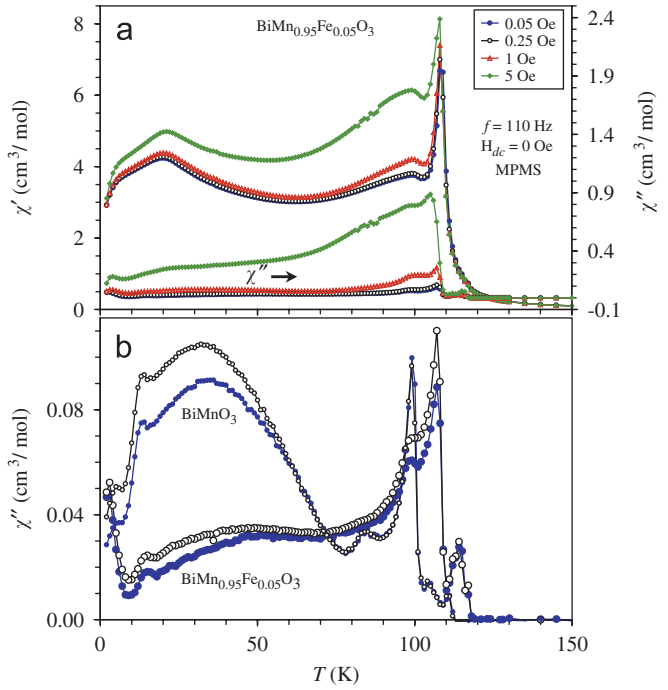


Fig. 6. (a) $\chi'$ vs $T$ and $\chi''$ vs $T$ curves of $BiMn_{0.95}Fe_{0.05}O_3$ measured at zero static magnetic field, frequency of 110 Hz, and different ac fields of 0.05, 0.25, 1, and $5\times10^{-4}$ T. (b) $\chi''$ vs $T$ curves of $BiMn_{0.95}Fe_{0.05}O_3$ (big circles) and $BiMnO_3$ (small circles) at $H_{ac}=5\times10^{-6}$ (dark circles) and $2.5\times10^{-5}$ T (white circles).

high frequency. It should be noted that the $\chi'$ vs $T$ and $\chi''$ vs $T$ curves of both $BiMn_{0.95}Fe_{0.05}O_3$ and $BiMnO_3$ show additional anomalies near 15 K (Fig. 6b: small peaks with sharp drop below 15 K) and near 4 K (Figs. 5 and 6: sudden decrease of $\chi'$ and peaks on $\chi''$). The origin of these anomalies and the anomalies near 20 K is not clear now. Probably they are related to changes in the domain dynamics. However, we note that the magnetic specific heat of $BiMnO_3$ plotted as $C_m/T$ vs $T$ also showed sharp drop below 15 K and weak curvature near 4 K [31].

Fig. 7 shows the specific heat of $BiMn_{0.95}Fe_{0.05}O_3$ at 0 and 9 T plotted as $C_p/T$ vs $T$ (the $C_p/T$ vs $T$ curve of $BiMnO_3$ at 0 T is given for the comparison). The measurement of the specific heat at 9 T shows a reduction of the specific heat as an almost constant shift on the $C_p/T$ vs $T$ curve between 2 and 50 K (the secondary axis of Fig. 7). According to the spin-wave theory the specific heat of a ferromagnet should reduce on applying a magnetic field due to the suppression of the thermal excitations of the spin wave [32]. The substitution of $Fe^{3+}$ for $Mn^{3+}$ also caused the reduction of the specific heat (see $(C_p(BiMnO_3)-C_p(BiMn_{0.95}Fe_{0.05}O_3))/T$ vs $T$ curve in Fig. 7). It can also be explained by the fact that the dilution of the Mn sublattice suppresses the excitations of the spin wave. On the other hand, the substitution of non-magnetic $Sc^{3+}$ for $Mn^{3+}$ resulted in the increase of the specific heat at low temperatures probably due to the enhanced contribution from spin-glass states [14].

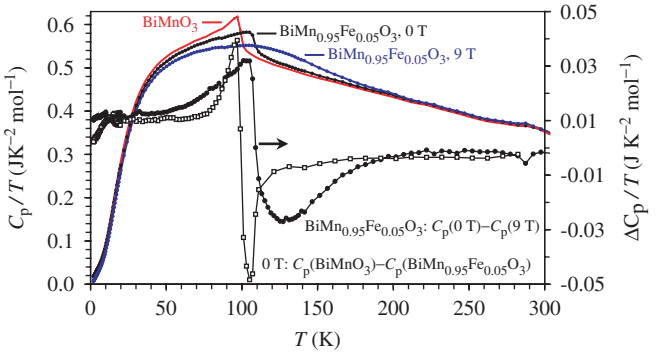


Fig. 7. $C_p/T$ vs $T$ curves of $BiMn_{0.95}Fe_{0.05}O_3$ at 0 and 9 T between 2 and 300 K. The $C_p/T$ vs $T$ curve of $BiMnO_3$ at 0 T (from Ref. [28]) is given for the comparison. The secondary axis shows the $(C_p(0\,T)-C_p(9\,T))/T$ vs $T$ curve for $BiMn_{0.95}Fe_{0.05}O_3$ and the $(C_p(BiMnO_3)-C_p(BiMn_{0.95}Fe_{0.05}O_3))/T$ vs $T$ curve.

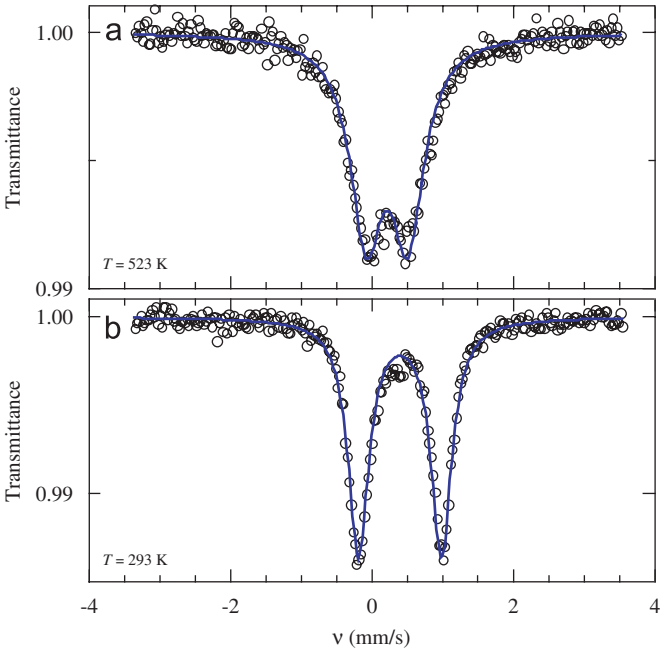


Fig. 8. Mössbauer spectra of $BiMn_{0.95}Fe_{0.05}O_3$ at (a) 523 K and (b) RT. Experimental data are shown by circles. Solid lines give the fitting curves.

$^{57}Fe$ Mössbauer spectra at various temperatures are shown in Figs. 8 and 9, and the fitting parameters are listed in Table 1. Fig. 10 gives the temperature dependence of the quadrupole splitting (QS) in $BiMn_{0.95}Fe_{0.05}O_3$ above RT. At RT, the isomer shift (IS) is an appropriate value for $Fe^{3+}$ ions. $BiMn_{0.95}Fe_{0.05}O_3$ is paramagnetic. There seems to be only one kind of $Fe^{3+}$ ions from the experimental observation of one doublet at RT and 523 K though there are two Mn sites in $BiMnO_3$ crystallographically [8]. Therefore, two Mn sites in $BiMnO_3$ cannot be seen by Mössbauer spectroscopy. The IS of $BiMn_{0.95}Fe_{0.05}O_3$ (0.40 mm/s) is close to that of $LaMn_{0.99}Fe_{0.01}O_3$ (IS = 0.38 mm/s) [20]. However, the QS of $BiMn_{0.95}Fe_{0.05}O_3$ (1.18 mm/s) is larger than that of $LaMn_{0.99}Fe_{0.01}O_3$ (QS = 1.09 mm/s) [20] in agreement with the larger $MnO_6$

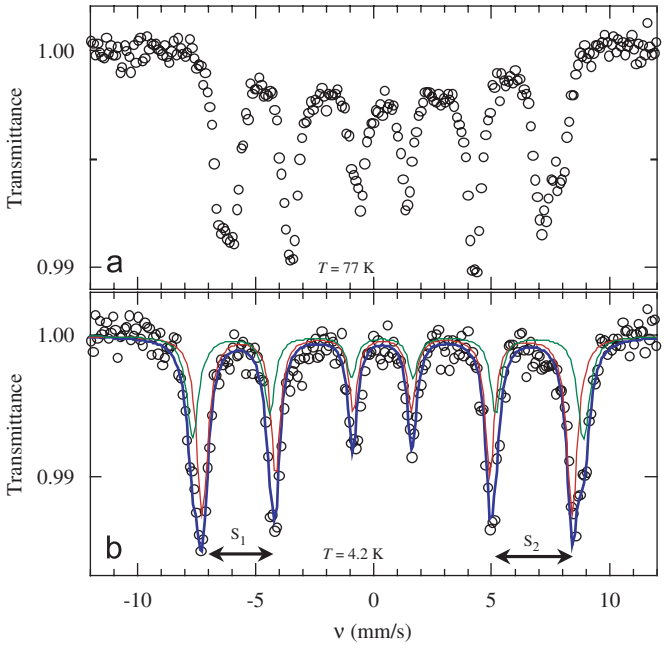


Fig. 9. Mössbauer spectra of $BiMn_{0.95}Fe_{0.05}O_3$ at (a) 77 K and (b) 4.2 K. Experimental data are shown by circles. Solid lines give the fitting curves.

Table 1
Mössbauer parameters of $BiMn_{0.95}$ $Fe_{0.05}O_3$ at various temperatures

| $T$ (K) | Component | IS (mm/s) | $H_{hf}$ (T) | QS (mm/s) | $\Gamma$ (mm/s) | Area (%) |
|---|---|---|---|---|---|---|
| 523 | | 0.22 | – | 0.59 | 0.55 | 100 |
| RT | | 0.40 | – | 1.18 | 0.35 | 100 |
| 4.2 | I | 0.51 | 48.7 | 0.42[a] | 0.57 | 75 |
| | II | 0.52 | 51.5 | 0.48[a] | 0.49 | 25 |

*Note*. IS: isomer shift (relative to α-Fe); $H_{hf}$: magnetic hyperfine field; QS: quadrupole splitting; $\Gamma$: full width at half maximum of the absorption line; area: relative area of the component.

[a] $S_2$–$S_1$ (see Fig. 9).

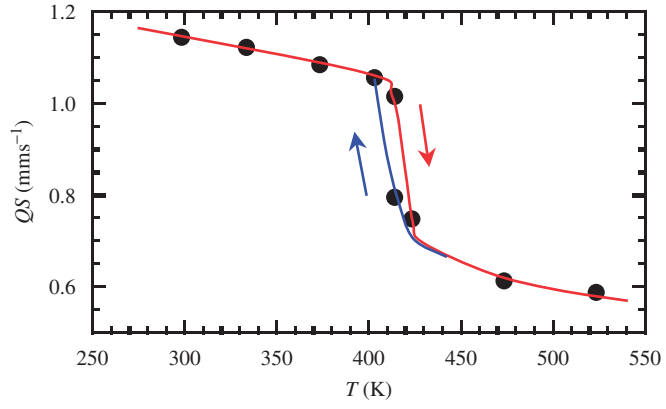


Fig. 10. Temperature dependence of the quadrupole splitting (QS) in $BiMn_{0.95}Fe_{0.05}O_3$ on heating and cooling. Experimental data are shown by circles. Solid lines are drawn for the eye. The quadrupole splitting is obtained by fitting the Mössbauer spectra with one doublet.

octahedra distortion in $BiMnO_3$ [8]. The distortion parameters ($10^4 \times \Delta$) of $MnO_6$ are 37.2 and 51.3 in $BiMnO_3$ [8] and 33.1 in $LaMnO_3$ [26]. The large QS of $BiMn_{0.95}Fe_{0.05}O_3$ and $LaMn_{0.99}Fe_{0.01}O_3$ can be explained by the strong Jahn-Teller distortions of $MnO_6$ octahedra and orbital ordering.

Above $T_{OO}$, the QS values show a step-like drop (Fig. 10). At 523 K, the QS value of $BiMn_{0.95}Fe_{0.05}O_3$ is reduced by almost two times compared with the RT value. This change is consistent with the occurrence of the structural transition at $T_{OO} = 414$ K that was interpreted as the orbital melting transition in the undoped $BiMnO_3$ ($T_{OO} = 474$ K) [8]. However, the presence of finite QS indicates that Jahn-Teller distortion remains (at least in one Mn site [8]) after melting the orbital order. This fact can explain the magnitude of the entropy change in the orbital order transition of $BiMnO_3$ and $BiMn_{0.95}Fe_{0.05}O_3$. Entropy change of $R\ln 3$ is expected if we consider the degree of freedom of three Jahn-Teller axes for each octahedron (a model of independent octahedra in Ref. [33]). On the other hand, taking into account constraints in the degrees of freedom for each octahedron, the entropy change was estimated to be 3.05 J/(mol K) [33] that is close to the experimental value for the undoped $BiMnO_3$. The finite QS above $T_{OO}$ is also in agreement with the structural data: $10^4 \times \Delta$ is 4.5 for the $Mn1O_6$ octahedron but it is 15.4 for the $Mn2O_6$ octahedron [8]. For example, in $LaMnO_3$ above $T_{OO}$, $10^4 \times \Delta$ is only 0.9 [26].

At 77 K, the spectrum is magnetically split indicating that the $Fe^{3+}$ ions are involved in the magnetic ordering. We can see two kinds of $Fe^{3+}$ ions, but the relative abundance is not 1:1 as expected crystallographically. Fitting was difficult because its background is curved and the peaks are broad. At 4.2 K, the spectrum decomposition was made assuming two components having broader peaks than those at RT.

The substitution of 5% of Fe must give rise to various surrounding configurations. If Fe–Mn and Fe–Fe interactions were also ferromagnetic (similar to the Mn–Mn interactions in $BiMnO_3$), the resulting magnetic situation could be simple. However, it will be complicated if the Fe–Mn and Fe–Fe interactions are antiferromagnetic as suggested from the decrease of saturation magnetization in $BiMn_{1-x}Fe_xO_3$.

It is reasonable to assume that the electronic state of an $Fe^{3+}$ ion depends strongly on the number of $Fe^{3+}$ ions around it. We can consider two cases, that is, the $Fe^{3+}$ ion has only $Mn^{3+}$ ions around it (configuration I) and the $Fe^{3+}$ ion has another $Fe^{3+}$ ion (configuration II). A simple calculation tells us that the ratio of these configurations is about 74:26 (I:II). Indeed, the two components at 4.2 K have a relative area ratio of 75:25 which is close to the naively expected value. That is, the component having a smaller $H_{hf}$ and the larger intensity corresponds to configuration I, and the component having a larger $H_{hf}$ and the smaller intensity corresponds to configuration II.

The anomalies in the $\chi$ vs $T$ curves at 0.01 T (Fig. 2) may result from local mixing of antiferromagnetic interactions. In other words, configuration II introduces magnetic frustration and interaction competition between neighbouring $Mn^{3+}$ ions.

The spectral broadening at low temperatures may be partially due to the multiplicity in the oriental relation between the three principal axes of the electric field gradient (efg) and the $H_{hf}$. Suppose a simple case that the efg is uniaxial. The peak positions change considerably depending on the azimuthal angle of the $H_{hf}$ relative to the unique axis of efg. Unfortunately, in this study, it is difficult to refer to the nature of efg exactly because the point symmetry is low at every Fe (Mn) site.

In conclusion, the properties of multiferroic $BiMn_{0.95}Fe_{0.05}O_3$ were studied in details by $^{57}Fe$ Mössbauer spectroscopy, dc and ac magnetization, specific heat, and DSC measurements. The large quadrupole splitting observed at 293 K in $BiMn_{0.95}Fe_{0.05}O_3$ can be explained by the strong Jahn-Teller distortion and cooperative orbital order. The finite quadrupole splitting above the orbital ordering temperature shows that Jahn-Teller distortion remains after melting the orbital order. This fact can explain the observation of resonant X-ray scattering reflections [7] above the orbital ordering temperature [34–36]. The substitution of 5% Fe for Mn in $BiMnO_3$ increases the temperatures of the structural monoclinic-to-orthorhombic phase transition and the ferromagnetic transition by about 10 K. On the other hand, the temperature of the monoclinic-to-monoclinic phase transition associated with the orbital ordering strongly decreases in $BiMn_{0.95}Fe_{0.05}O_3$.

## Acknowledgment

This work was partly supported by the Grants-in-Aid for Scientific Research grant no. 17105002 from the Ministry of Education, Culture, Sports, Science, and Technology MEXT of Japan.

## References

[1] F. Sugawara, S. Iiida, Y. Syono, S. Akimoto, J. Phys. Soc. Jpn. 25 (1968) 1553.
[2] A. Moreira dos Santos, A.K. Cheetham, T. Atou, Y. Syono, Y. Yamaguchi, K. Ohoyama, H. Chiba, C.N.R. Rao, Phys. Rev. B 66 (2002) 64425.
[3] T. Kimura, S. Kawamoto, I. Yamada, M. Azuma, M. Takano, Y. Tokura, Phys. Rev. B 67 (2003) 180401(R).
[4] R. Ramesh, N.A. Spaldin, Nat. Mater. 6 (2007) 21.
[5] D.I. Khomskii, J. Magn. Magn. Mater. 306 (2006) 1.
[6] T. Atou, H. Chiba, K. Ohoyama, Y. Yamaguchi, Y. Syono, J. Solid State Chem. 145 (1999) 639.
[7] C.H. Yang, J. Koo, C. Song, T.Y. Koo, K.B. Lee, Y.H. Jeong, Phys. Rev. B 73 (2006) 224112.
[8] A.A. Belik, S. Iikubo, T. Yokosawa, K. Kodama, N. Igawa, S. Shamoto, M. Azuma, M. Takano, K. Kimoto, Y. Matsui, E. Takayama-Muromachi, J. Am. Chem. Soc. 129 (2007) 971.
[9] Z.H. Chi, C.J. Xiao, S.M. Feng, F.Y. Li, C.Q. Jin, X.H. Wang, R.Z. Chen, L.T. Li, J. Appl. Phys. 98 (2005) 103519.
[10] E. Montanari, G. Calestani, A. Migliori, M. Dapiaggi, F. Bolzoni, R. Cabassi, E. Gilioli, Chem. Mater. 17 (2005) 6457.
[11] R.J. Goff, J.P. Attfield, J. Solid State Chem. 179 (2006) 1369.
[12] A.A. Belik, E. Takayama-Muromachi, Inorg. Chem. 46 (2007) 5585.
[13] M. Azuma, H. Kanda, A.A. Belik, Y. Shimakawa, M. Takano, J. Magn. Magn. Mater. 310 (2007) 1177.
[14] A.A. Belik, T. Yokosawa, K. Kimoto, Y. Matsui, E. Takayama-Muromachi, Chem. Mater. 19 (2007) 1679.
[15] I.A. Santos, H.L.C. Grande, V.F. Freitas, S.N. de Medeiros, A. Paesano Jr., L.F. Cotica, E. Radovanovic, J. Non-Crystal. Solids 352 (2006) 3721.
[16] C.F. Chung, J.P. Lin, J.M. Wu, Appl. Phys. Lett. 88 (2006) 242909.
[17] I. Sosnowska, W. Schaffer, W. Kockelmann, K.H. Andersen, I.O. Troyanchuk, Appl. Phys. A-Mater. Sci. Process. 74 (2002) S1040.
[18] (a) C.H. Yang, J.H. Song, H.J. Lee, S. Yoon, T.Y. Koo, Y.H. Jeong, Phys. Status Solidi B 241 (2004) 1453;
(b) C.H. Yang, T.Y. Koo, Y.H. Jeong, Solid State Commun. 134 (2005) 299.
[19] K. Takahashi, M. Tonouchi, Jpn. J. Appl. Phys. 45 (2006) L755.
[20] M. Pissas, A. Simopoulos, J. Phys.: Condens. Matter 16 (2005) 7419.
[21] M. Kopcewics, V.A. Khomchenko, I.O. Troyanchuk, H. Szymczak, J. Phys.: Condens. Matter 16 (2005) 4335.
[22] A. Urushibara, Y. Moritomo, T. Arima, A. Asamitsu, G. Kido, Y. Tokura, Phys. Rev. B 51 (1995) 14103.
[23] A.J. Millis, B.I. Shraiman, R. Mueller, Phys. Rev. Lett. 77 (1996) 175.
[24] B.B. Van Aken, O.D. Jurchescu, A. Meetsma, Y. Tomioka, Y. Tokura, T.T.M. Palstra, Phys. Rev. Lett. 90 (2003) 066403.
[25] T. Okuda, A. Asamitsu, Y. Tomioka, T. Kimura, Y. Taguchi, Y. Tokura, Phys. Rev. Lett. 81 (1998) 3203.
[26] J. Rodríguez-Carvajal, M. Hennion, F. Moussa, A.H. Moudden, L. Pinsard, A. Revcolevschi, Phys. Rev. B 57 (1998) 3189(R).
[27] J.S. Zhou, J.B. Goodenough, Phys. Rev. B 60 (1999) 15002(R).
[28] Y. Murakami, J.P. Hill, D. Gibbs, M. Blume, I. Koyama, M. Tanaka, H. Kawata, T. Arima, Y. Tokura, K. Hirota, Y. Endoh, Phys. Rev. Lett. 81 (1998) 582.
[29] F. Izumi, T. Ikeda, Mater. Sci. Forum. 321−324 (2000) 198.
[30] A.A. Belik, N. Tsujii, H. Suzuki, E. Takayama-Muromachi, Inorg. Chem. 46 (2007) 8746.
[31] A.A. Belik, E. Takayama-Muromachi, Inorg. Chem. 45 (2006) 10224.
[32] L.J. de Jongh, A.R. Miedema, Adv. Phys. 50 (2001) 947.
[33] M.C. Sanchez, G. Subias, J. Garcia, J. Blasco, Phys. Rev. Lett. 90 (2003) 045503.
[34] R. Colella, Q. Shen, Acta Crystallogr. Sec. A 62 (2006) 459.
[35] Q. Shen, I.S. Elfimov, P. Fanwick, Y. Tokura, T. Kimura, K. Finkelstein, R. Colella, G.A. Sawatzky, Phys. Rev. Lett. 96 (2006) 246405.
[36] G. Subias, J. Herrero-Martin, J. Garcia, J. Blasco, C. Mazzoli, K. Hatada, S. Di Matteo, C.R. Natoli, Phys. Rev. B 75 (2007) 235101.